Direct search dark matter experiments strive to control backgrounds sufficiently so as to achieve an expected rate of less than 1 background event recorded in the anticipated exposure time and target mass, essentially that we have zero background within the fiducial volume. An assumption that this is achievable for all the directional technologies compared here was an important caveat made in the previous section of this work. This next section now addresses the realities of this assumption. Specifically we seek to answer the question firstly whether or not directional low pressure gas TPCs can in principle achieve such low backgrounds at the experiment scale required to reach the proposed scientific goals, but further, whether particular TPC readout technologies, with their individual associated intrinsic backgrounds and discrimination capabilities, are more or less able to reach these goals. The latter aspect depends in part on assumptions about the radio-purity of internal detector materials likely involved, most notable for instance because this affects the total internal neutron background. So an alternative tack, adopted here also, is to estimate and compare the specification on material radio-purity required for success, for instance the ^{238}U content in each case, then to comment on the achievability of these requirements.

As shown in [ref x, Abbassi 2005] the additional particle identification properties of directional detectors mean that in principle they may in actuality be able to tolerate a non-zero level of isotropic nuclear recoil background, yet still be able to identify the signal of interest here for dark matter, a non-isotropic distribution of recoil directions. However, the level of tolerance will depend strongly on the capabilities of the technology and anyway will clearly reduce sensitivity overall. A maximum signal to background ratio of order 10 might be a reasonable upper limit in certain circumstances [ref ?]. Nevertheless, a good starting point for comparison purposes, adopted for this work, is to assume an aim of zero background.

The following sections present results and conclusions on these issues based on new Geant4 detector Monte-Carlo simulations of the various key background contributions. Although not necessarily mandatory, experience from many dark matter experiments demonstrates that full fiducialisation of the active detector volume is likely necessary to achieve the background goals. This aspect is addressed in 0.1. The fundamental issue of the neutron background, which results in nuclear recoil events likely indistinguishable from WIMP induced events, is addressed in 0.2, considering separately contributions from cosmic ray muon neutrons, and rock and detector neutrons. The subsequent parts cover respectively simulations of gamma, radon related backgrounds. For the majority of the technologies some generic conclusions can be drawn based on the commonality of the basic infrastructure needed for any TPC dark matter experiment, such as a deep site, passive shielding and containment vessel. The majority of any variance from this comes from details of the internal TPC structures, notably the readout planes. These aspects are together summarized in 0.6.

0.1 Fiducialization

0.2 Neutron Backgrounds

Neutrons are a major concern for all direct search experiments because they can produce nuclear recoils just like WIMPs. However, there are various issues that make the requirements for mitigating against neutron backgrounds in a low pressure gas TPC significantly different from those cases involving conventional solid or liquid based detector technologies. Firstly, the potentially low sensitivity to light charged particles, muons, muon-induced secondary particles and electrons, means that these may not be recorded. Secondly, the low density of the target means neutrons are less likely to undergo double or multiple scatters. Both these factors potentially reduce options for vetoing neutron induced nuclear recoils, depending on the readout technology chosen. The former does depend critically on the degree of position segmentation of the readout and the energy threshold achievable in those individual readout channels, essentially the sensitivity to dE/dx. The issue of vetoing by recording multiple neutron scatters then depends on the contiguous size of the detector array. For instance, at 200Torr SF_6, the mean free path of a typical background neutron is 60m. This would be the sort of scale required to have any benefit from detection of multiple neutron scatters.

Factors such as these, the uniqueness of the low pressure TPC technique and potentially powerful particle identification, mean that estimating neutron backgrounds by extrapolation from existing background simulations such as have been performed for massive xenon or bolometric detectors [Aprile 2013, arxiv 1306.2303v2 has a good description for XENON100], is not appropriate. The work presented here is thus based on a set of dedicated TPC Monte-Carlo simulations. Some relevant initial work on neutron backgrounds was previously undertaken by some of the authors here but focused on smaller TPC target masses of order $1-10$kg [This is the Cygnus24 paper ?]. The new work presented here makes use of the latest updated Geant4 and SOURCES packages and specifically targets the more complex situation of neutron background mitigation in the much larger experiments required to reach the goals of CYGNUS. As noted the procedure adopted is to start by examining aspects that are independent of the internal readout technology. This includes firstly the laboratory location, determined by the depth, rock composition and cavern geometry. Secondly, the outer passive shielding and any active veto system, and finally the containment vessel, modeling both its geometry and composition. The remit here is to investigate muon-induced neutrons resulting from cosmic-rays penetrating from the Earth's surface and also neutrons produced by spontaneous fission and alpha-n reactions in the rock and shielding/vessel materials. The procedure thus requires simulation of the geometry, particle production, tracking and detection, the goal being to find the rate of neutron-induced nuclear recoils anticipated in different situations. From this can be determined requirements for such issues as the amount of passive shielding, the efficiency and form of any external veto and the form and purity of the vessel materials, such as required to achieve the goal of zero background. The issue of neutrons from internal detector components, that depends on details of the readout technology, is addressed last.

0.2.1 Laboratory and TPC Geometry

Most parameters are independent of the location of the experiment, especially regarding the inner parts of the detector. Other parameters can be scaled to estimate the rate of background events at different laboratories. For these simulations, we concentrate on the background present in salt rock similar to the Boulby Underground Laboratory in the UK.

In the case of neutrons from (α, n) and spontaneous fission emanating from the rock, 3m of material were simulated on each side of the detector. As presented in 1, simulations have shown that the neutron flux saturates at this distance so neutrons produced beyond 3m do not actively contribute to the total neutron flux. For muon-induced neutrons, the thickness of rock is increased to 20m in order to fully allow the muons created at the surface of the geometry to decay.

In both case, it was assumed that no objects other than the vessel and its shielding are present in the cavern. The dimension of the vessel, however, depends on the materials from which it is made and the composition and pressure of the gas adopted for the experiment of which there are many possibilities. For the purposes of making broad comparisons here, bearing in mind the science goals of CYGNUS, it was decided to assume use of SF_6 gas at 50Torr with volume sufficient to produce around 0.5Ton of target nuclei, in this case of fluorine. In both case, a generic detector with an inner-volume of $10 \times 10 \times 10\mathrm{m}^3$ was modeled. Real vacuum vessels of such size will require strengthening supports both inside and outside. However, for simplicity in simulations the mass of these was taken into account by applying an appropriate average increase in thickness to the vessel walls.

As stated, the background from internal TPC components will be affected by details of the readout design, covered later. Nevertheless, some generic assumptions can be made about other TPC structures required inside the detector which are likely common to any design. Most notable here is the central cathode and field cage. However, we note that the total area required for the former will also depend on the gas mixture adopted, since this influences the diffusion and hence determines the maximum drift distance that can be tolerated. For the comparisons here we assume a compromise drift distance of 50cm, which yields a total cathode area of $2000\mathrm{m}^2$ in both options. The design of this is assumed here to comprise ultra-thin cathode sheets supported on acrylic frames. The field cage itself can also be made of light acrylic components, with copper strips to act as the field rings. In these components the acrylic provides by far the dominant mass, conservatively estimated to be 86.4 tons [1000xDRIFT]. The components are, in turn, approximated as sheets of appropriate thickness in the TPC to simulate their neutron yield. The thickness of the sheets is chosen such that it may account for self-shielding. Geant4 provides the option of homogeneously populate the material studied with the relevant primary particles. This option enables the simultaneous treatment of background originating from the bulk of materials,

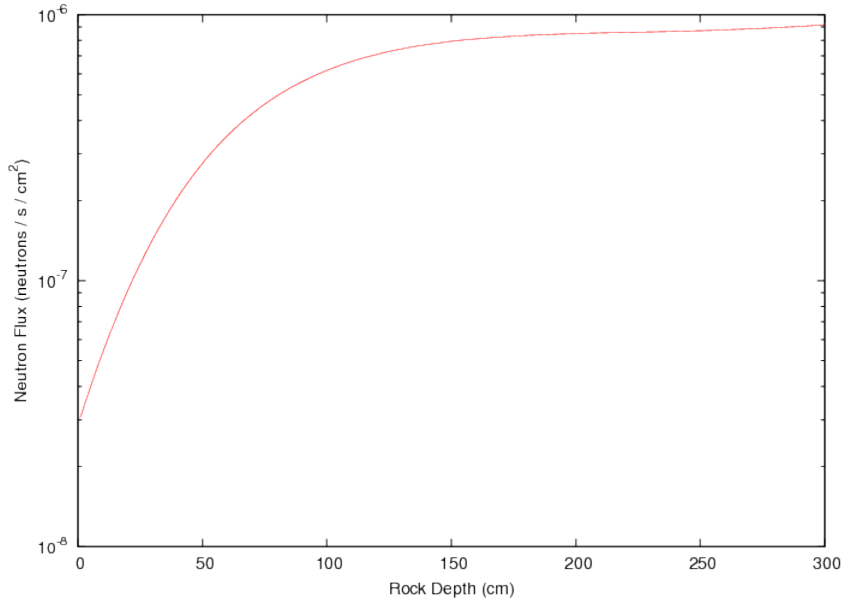

Figure 1: Rock neutron flux at Boulby as a function of depth

as well as surface background contamination.

0.2.2 Rock Neutrons and Passive Shielding

The first simulations were performed to determine what thickness of passive neutron shielding is required around the CYGNUS detector to ensure an induced recoil rate from this source that is below 1 per year. It is recognized that an active veto shield is also likely needed to assist with rejection of muon related neutrons (see 0.2.5) and that, in practice, this could be fully, or partially, integrated with the passive shield. The simulation varies the thickness of a water shield around all sides of the detector until the requirement of less than 1 background event per live-year is fulfilled. Possible contamination of the water by radionuclei was not simulated as measurement performed at Boulby for DRIFT showed that the level of contamination in clean, non-distilled water were on par with the levels already obtained with polypropylene pellets. Furthermore, it is assumed here that any containment structure or internal components, such as photomultipliers, are of sufficiently low background and low mass to be ignored. We note also that account needs to be taken of the energy threshold chosen, as determined in part by the science priorities. To allow for this we consider cases for a 1 and 10keV threshold.

For this work, SOURCES was used to generate neutrons from the U and Th decay chains in salt rock corresponding to the Boulby Underground Laboratory. The results obtained in this section can be scaled to different underground laboratories and additional shielding materials can always be added if required. SOURCES simulates the contribution to the ^{238}U chain from spontaneous fission using the Watt spectrum, while the (α, n) spectra are computed from the energy of the alphas and the related cross-sections, branching ratios for the different transitions between excited states, lifetimes of the isotopes and stopping power of the alphas in the modeled materials. The version of SOURCES used has been modified to extend the energy range considered from up to 6.5MeV originally to up to 10MeV using experimental data [Quote Carson ?].

2 shows the neutron energy spectra obtained for both decay chains at Boulby. We used Geant4 to randomly populate

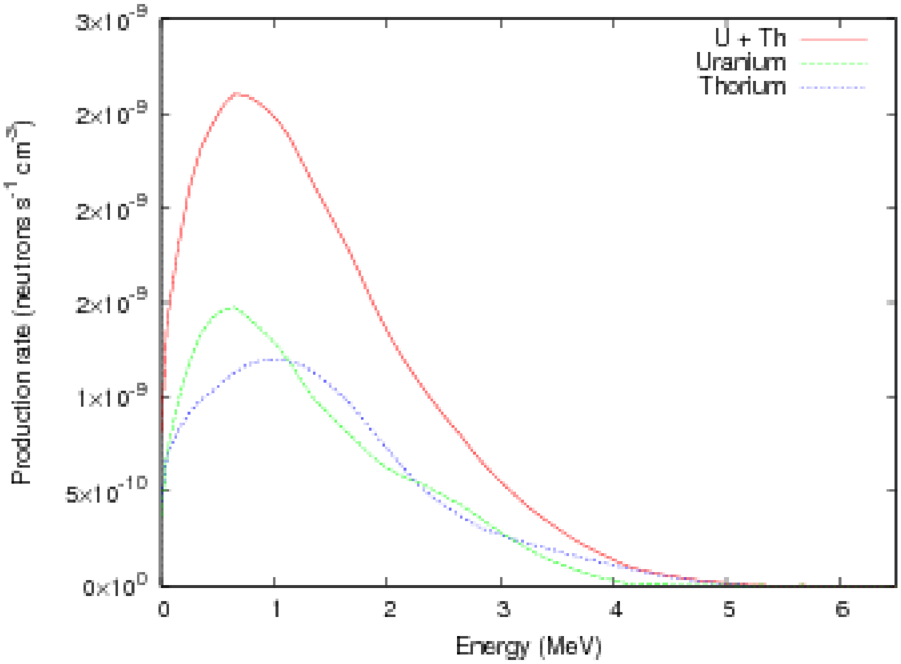

Figure 2: Neutron energy spectrum from the salt rock at Boulby

the rock with isotropic neutrons with energy sampled from the sum of spectra obtained with SOURCES. The simulation was repeated for various thickness of the water shield until the nuclear recoil rate in the gas was below the imposed limit. The results obtained are summarised in Table1. Similar tests with Geant4 carried out by the authors have shown that there exists a linear relationship between the nuclear recoil rate in the detector and the pressure of the target gas so long the probability of double scattering of neutrons in the gas remains negligible. We have found this relationship to be true only for nuclear recoils. On the other hand, simulations of Compton scattering at different pressures have shown evidence for self-shielding from the gas at high pressure. To reduce the computational burden, simulations of the rock background were done at 600Torr, a factor 12 above the chosen pressure. We made sure that simulations performed at both the increased and nominal pressure indeed returned the same results. This shortcut is possible since low pressure gas TPCs can be made insensitive to gammas by increasing their threshold such that the lower dE/dx of electron recoils do not trigger the analysis. In each case, a separate simulation dedicated to the gamma background was performed at nominal pressure.

1 shows that 75cm of water shielding are required in order to reduce the neutron background in salt rock below 1 event per year. The concentration assumed were 70ppb $\left({}^{238}\mathrm{U}\right)$ and 125ppb $\left({}^{232}\mathrm{Th}\right)$ as reported in [Murphy, IDM2004]. We found that 70ppb of ^{238}U produced 3.5×10^{-8}neutrons/s/cm^3 with a mean energy of 1.74MeV, and that 125ppb of ^{232}Th produced 3.08×10^{-8}neutrons/s/cm^3 with a mean energy of 1.92MeV.

0.2.3 Vessel Neutrons

As seen in 0.2.2, the external rock neutron flux can be controlled by passive shielding. Neutrons from internal detector radioactivity are known to be a harder challenge since control of this likely relies on selecting radio-pure materials, use of tricky internal shielding or innovative analysis techniques. The vacuum vessel, being the component with by far the

Water shield thickness	Nuclear recoil rate in salt rock
50cm	$(1.8 \pm 0.7) \times 10^{-6}$Hz
75cm	$\leq 2.96 \times 10^{-8}$Hz (90%CL)

Table 1: Nuclear recoil rates from rock neutrons above a $1\mathrm{keV_r}$ threshold as a function of shield thickness in salt rock

	$1\mathrm{keV_r}$ threshold		$10\mathrm{keV_r}$ threshold	
shield thickness	U (ppb)	Th (ppb)	U (ppb)	Th (ppb)
0cm	$(4.910 \pm 0.004) \times 10^{-3}$	$(2.455 \pm 0.002) \times 10^{-3}$	$(6.537 \pm 0.006) \times 10^{-3}$	$(3.269 \pm 0.003) \times 10^{-3}$
10cm	$(2.709 \pm 0.007) \times 10^{-2}$	$(1.354 \pm 0.004) \times 10^{-2}$	$(3.96 \pm 0.01) \times 10^{-2}$	$(1.983 \pm 0.006) \times 10^{-2}$
20cm	$(8.1 \pm 0.1) \times 10^{-1}$	$(4.05 \pm 0.06) \times 10^{-1}$	1.14 ± 0.02	$(5.7 \pm 0.1) \times 10^{-1}$

Table 2: Maximum concentration of ^{238}U and ^{232}Th for a steel vessel with internal acrylic shielding

largest mass, has the potential to dominate this aspect, followed by the outer passive shield, TPC field cage, and resistors. Rather than assume values for the U and Th content of the vessel materials the approach taken here is to determine from the simulations what amount of U, Th contamination can be tolerated in the vessel without compromising the criteria of less than one event recorded per year, at each energy threshold. Given the potential difficulty of obtaining steel with low U, Th content, the simulation also considers acrylic and titanium vessels. For the steel and titanium vessels, we explore the possibility of including acrylic shielding inside the vessel to block neutrons emanating from the vessel. In this case, the acrylic inner-shield is assumed to be inert, but its neutron yield can be estimated from the simulation of an acrylic vessel. In order to deduce the maximum U and Th content possible, it is necessary to fix the ratio of the two. We used the UKDM database [ref of UKDM] to estimate the typical ratio of U to Th. This ratio seemed to vary greatly between samples, especially in the case of steel. In these situations, we chose a ratio which would correspond to a typical case, or to a known example. As such, a ratio of $\mathrm{C_U} = 2\mathrm{C_{Th}}$ was assumed for steel, roughly similar to the ratio in the DRIFT vessel stainless steel. In any case, these results should be considered as benchmark values in order to estimate the feasibility of building a large dark matter TPC detector rather than a full background simulation. Secular equilibrium is assumed for both the U and Th decay chains. Tables 2 and 3 summarise the results in terms of specifications on the maximum U, Th levels that can be tolerated in each scenario in order to obtain less than one nuclear recoil per year..

Some initial conclusions can be extracted from these results. Firstly, a large radio-assay was conducted for the LZ experiment [ref LZ paper] when several samples of steel were examined. Low-background concentrations were achieved at 0.08ppb ^{238}U and 0.12ppb ^{232}Th. This is a factor 10 improvement for U and 5 for Th compared to the DRIFT vessel (0.81ppb U and 0.51ppb Th) [ref UKDM]. However, similar concentrations were achieved in stainless steel by the GERDA group (0.081ppb U and 0.37ppb Th) [Ref Gerda paper]. The simulation shows a slightly larger tolerance for contaminated steel than for titanium, this is because SOURCES predicts a higher neutron mean energy in titanium. To our knowledge, no efforts to develop steel with contamination levels on the order of 10^{-4}ppb have been fructuous so steel vessels without

	$1\mathrm{keV_r}$ threshold		$10\mathrm{keV_r}$ threshold	
shield thickness	U (ppb)	Th (ppb)	U (ppb)	Th (ppb)
0cm	$(8.54 \pm 0.02) \times 10^{-4}$	$(1.422 \pm 0.003) \times 10^{-3}$	$(9.86 \pm 0.02) \times 10^{-4}$	$(1.644 \pm 0.003) \times 10^{-3}$
10cm	$(9.95 \pm 0.06) \times 10^{-3}$	$(1.66 \pm 0.01) \times 10^{-2}$	$(1.30 \pm 0.01) \times 10^{-2}$	$(2.16 \pm 0.01) \times 12^{-2}$
20cm	$(1.73 \pm 0.03) \times 10^{-1}$	$(1.73 \pm 0.03) \times 10^{-1}$	$(1.33 \pm 0.03) \times 10^{-1}$	$(2.21 \pm 0.05) \times 10^{-1}$

Table 3: Maximum concentration of ^{238}U and ^{232}Th for a titanium vessel with internal acrylic shielding

internal shielding may not be a viable option for detectors of the size of CYGNUS. Regarding Titanium, the lowest concentrations reported in the LZ background assay [Ref LZ paper] are 7.29×10^{-3}ppb U and 5.66×10^{-2}ppb Th. These figures place the need for acrylic internal shielding slightly above 10cm. A steel vessel would require slightly more than 10cm of internal acrylic shielding, but given the small difference, the prohibitive cost of titanium may be an advantage to stainless steel vessels.

Finally, we turn our attention to designs based on acrylic vessel. This simulation can both test the viability of acrylic vessels and the effectiveness of the acrylic internal shield mentioned above. Indeed, the steel and titanium designs rely on the assumption that the contribution of the internal shield to the neutron flux would be negligible. The simulation of a 47 tonnes acrylic vessel shows a maximum concentration of $(6.607 \pm 0.004) \times 10^{-3}$pbb with a 1keV threshold and $(9.301 \pm 0.007) \times 10^{-3}$pbb with a 10keV threshold. These numbers are comparable to the radio-purity achieved in acrylic with SNO+, 2.35ppt ^{238}U and 9.60ppt ^{232}Th [ref SNO+ paper (Neil's email 21/10/16)].

Different vessel designs made of steel, titanium and acrylic have been compared. We showed that both steel and titanium, assuming the best concentrations of radio-nuclei available in the literature, require the addition of about 10cm of acrylic internal shielding in order to bring the nuclear recoil rate below one per year. In the case of a steel or titanium vessel, the additive contributions of the vessel and its inner shield to the neutron background would require that the concentrations of the different radio-nuclei be well below the maximum figures quoted in 2 and 3. We conclude that acrylic vessels are the preferred option in terms of managing the background levels.

0.2.4 TPC read-out neutrons

Many of the current directional detectors [need ref to each one] have been built around different read-out technologies. In this section, we investigate the neutron background from the main materials used in each read-out. While backgrounds from the rock and the vessel are expected to dominate due to their relative size, the detector cannot be shielded from neutrons produced by the read-out materials. This and the large volume of CYGNUS make the careful selection of read-out materials an important part of the design process. In this section, we only explore the background level of the read-out, the comparison of their directional sensitivity is discussed in 0.6. For each material examined, we used SOURCES to estimate the neutron production rate for ^{238}U and ^{232}Th. We then simulated neutrons sampled from each spectra separately using Geant4 to obtain a separate figure for both decay chains. Similarly to the vessel background simulation, we fixed the U to Th ratio based on materials listed in [ref UKDM databank]. The simulated neutrons are produced in a sheet of the studied material placed inside the gas volume of the CYGNUS detector. The thickness of the sheet is chosen to resemble the typical thickness of the material simulated. For example, for the simulation of neutrons from ceramics, the thickness of the simulated sheet of ceramic was that of a resistor. From the results, we calculate the maximum concentration of ^{238}U and ^{232}Th per grams of material such that the neutron background from this material is less than 1 event per year with a threshold at either 1 or 10keV$_\mathrm{r}$.

Firstly, we investigate the Micro Pixel Chamber (μ-PIC) readout as used in NEWAGE [ref NEWAGE + arXiv:hep-ex/0301012v2 for m uPICS]. The μ-PIC is constituted of a double sided circuit board separated by 100μm thick polymide substrate. Typical ^{238}U and ^{232}Th concentrations in the polymide measured by the NEWAGE collaborations are 1.2ppm ^{238}U and 5.8ppm ^{232}Th. 4 shows the results of the simulation for the $\mu-$PIC polymide. Based on an 0.8mm thick polymide and a drift distance of 50cm, the total mass of polymide can be estimate as roughly 2.2Ton corresponding to a maximum concentration on the order of 5.27×10^{-3}ppb for ^{232}Th and 1.05×10^{-3}ppb for ^{238}U.

The combination of pixel and Gas Electron Multipliers (GEMs) have been investigated as possible read-out for a TPC dark matter detector [Ref D3 arXiv:1110.3401 and UNM arXiv:1510.02170]. GEMs are composed of two sheets of copper separated by ~0.4mm of kapton. Radio-pure copper can be manufactured with U and Th levels below 0.1ppb [Ref UKDM], but the concentration of these isotopes in kapton is about 8ppb ^{232}U and 9ppb ^{232}Th [Ref UKDM]. The results of the simulation are shown in 5 for copper and 6 for kapton. Assuming a 10μm thick copper coating on each GEM, we estimate the amount of copper for the whole detector to be around 179kg. The corresponding maximum concentration allowed is

Threshold	Concentration of 232-Th per gram (ppb/g)	Concentration of 238-U per gram (ppb/g)
1keV	$(9.35 \pm 0.02) \times 10^3$	$(1.870 \pm 0.004) \times 10^3$
10keV	$(1.182 \pm 0.003) \times 10^4$	$(2.363 \pm 0.005) \times 10^3$

Table 4: Maximum allowed concentrations of ^{238}U and ^{232}Th per grams of polymide in $\mu -$ PIC read-outs.

Threshold	Concentration of 232-Th and 238-U per gram (ppb/g)
1keV	$(5.6 \pm 0.1) \times 10^4$
10keV	$(7.3 \pm 0.2) \times 10^4$

Table 5: Maximum allowed concentrations of ^{238}U and ^{232}Th per grams of copper in GEMs read-out.

0.32ppb for both U and Th with a 1keV threshold, and 0.41ppb with a 10keV threshold. We found these numbers to be acceptable as many copper samples measured in [REF UKDM] have contamination levels below these values. For kapton however, estimations based on 1.14Ton corresponding to a thickness of kapton of 0.4μm inside the GEMs, the maximum concentrations allowed are $2.27\,(2.86) \times 10^{-2}$ppb with a 1keV (10keV) threshold for both isotopes. These values are well below the current measured concentrations so a careful material selection will be necessary for this read-out.

A wire based read-out such as the one used in the DRIFT detector [REF any drift or Carson] has two main sources of background. Ceramics from resistors are known to have high U and Th concentrations, with typical values around 500ppb ^{238}U and 2000ppb ^{232}Th. The amount of radio-isotopes can vary by a large amount depending on the batch, brand or type of resistors, so the numbers used are purposely chosen to be slightly high. Furthermore, its is assumed that aluminium oxides are the main neutron emitters in resitors. Another potential source of neutrons is the steel making the wires of the MWPCs. The results for ceramics are summarized in 7, and the values for steel are shown in 8.

Using the DRIFT detector as an example, we estimated 1.94g of steel per meter cubed TPCs. This roughly corresponds to 3.9kg of steel for CYGNUS and the associated maximal contamination levels are 22.1(28)ppb for ^{232}Th with a 1(10)keV threshold and 44.2(56.1)ppb for ^{238}U with similar thresholds. This is well below the measured 5ppb $\left(^{232}\text{Th}\right)$ and 1.5ppb $\left(^{238}\text{U}\right)$ measured for the grid wires of the DRIFT-I vessel [ref UKDM]. Using again the DRIFT detector as an example, we estimated the quantity of ceramics as 22.6g per meter cubed TPCs [ref Carson], the corresponding maximum concentrations allowed for Cygnus are $5.31\,(6.73) \times 10^{-1}$ppb for ^{232}Th and $1.33\,(1.68) \times 10^{-1}$ppb for ^{238}U using the usual thresholds. These values are well below the 500ppb ^{238}U and 2000ppb ^{232}Th found in typical resistors.

In this section, we looked at the neutron background from (α, n) reactions and spontaneous fission from read-out materials used by the current direct detection experiments. While some materials met the background requirement of the CYGNUS detector, it seems no read-out technology is, in their current state, able the satisfy the CYGNUS background criteria. An important developmental step for CYGNUS will be to either perform extensive material screening in order to select only materials with the lowest amount of U and Th or to develop new ways to install the read out planes so as to minimise the amount of materials required.

Threshold	Concentration of 232-Th and 238-U per gram (ppb/g)
1keV	$(2.60 \pm 0.03) \times 10^4$
10keV	$(3.27 \pm 0.04) \times 10^4$

Table 6: Maximum allowed concentrations of ^{238}U and ^{232}Th per grams of kapton in GEMs read-out.

Threshold	Concentration of 232-Th per gram (ppb/g)	Concentration of 238-U per gram (ppb/g)
1keV	$(1.200 \pm 0.001) \times 10^4$	$(3.001 \pm 0.003) \times 10^3$
10keV	$(1.522 \pm 0.002) \times 10^4$	$(3.804 \pm 0.004) \times 10^3$

Table 7: Maximum allowed concentrations of ^{238}U and ^{232}Th per grams of ceramic in MWPCs read-out.

Threshold	Concentration of 232-Th per gram (ppb/g)	Concentration of 238-U per gram (ppb/g)
1keV	$(8.57 \pm 0.05) \times 10^4$	$(1.714 \pm 0.009) \times 10^5$
10keV	$(1.088 \pm 0.006) \times 10^5$	$(2.176 \pm 0.001) \times 10^5$

Table 8: Maximum allowed concentrations of ^{238}U and ^{232}Th per grams of steel in MWPCs read-out.

0.2.5 Muon-induced neutrons and active vetoing

For the case of muon-induced neutrons, the muon energy spectrum and its angular distribution was simulated using the MUSUN simulation [ref Vitaly MUSUN paper]. MUSUN takes into account the angular profile and the composition of the rock overburden for the transportation of cosmic ray muons. The output is an array of the muon energies, positions and momenta. This array is inputted into the Geant4 simulation which simulates the final meters of the particles in the rock. The simulation allows for at least 20m of rock on each side of the detector to give each muon ample space to interact.

More than 200 million muons were simulated at the surface of the rock volume. A muon-veto was placed in the simulation outside of the external water shielding. The muon-vetos were represented as 1cm thick sheets of plastic scintillator placed on top of the detector and on each lateral sides. No muon-veto was placed below the detector. Muons entering these volumes are recorded in the simulation and latter used to veto nuclear recoils in the gas volume using coincidence of events. Similarly, the analysis searches for double nuclear scattering or electron recoils above the 1keV threshold recorded in the gas with a matching event number. There events are rejected as their are not WIMP candidate events. Using electron recoils as a way to veto nuclear recoils requires the simulation to be carried at nominal pressure. If this method is not used, the pressure can be increased but we found that in this configuration, the nuclear recoil rate is largely above 1/year. Since many muons are produced with energies on the TeV scale as seen in 3, we found that some events are recorded with recoil energies larger than what would be expected for a WIMP recoil. For this simulation, we explicitly limited the analysis to a region of interest situated between 1 and $100\mathrm{keV_r}$.

Muons passing the rock-cavern boundary are recorded in order to calculate the equivalent duration of the Monte-Carlo simulation. The number of muons recorded is compared to the measured value of the muon flux at the Boulby Underground Laboratory, $(4.09 \pm 0.15) \times 10^{-8}\mathrm{cm}^{-2}/\mathrm{s}^{-1}$, corresponding to a vertical rock overburden of 2805 ± 45m.w.e.. Using this technique, we found that the simulation correspond to $(2.8 \pm 0.1) \times 10^7$s, during which no events were seen in the region of interest, leading to an upper-limit on the rate of muon-induced neutron nuclear recoil rate of 8.71×10^{-8}Hz.

0.2.6 Conclusion of neutron background

In the previous sections, we simulated the neutron background from the main sources. We saw that the external neutron background can easily be reduced by the use of a low-Z shielding material. For muon-induced neutrons, an excellent rejection rate can be achieved when combining an external muon veto and an analysis of coincidence between events in the gas. Many dark matter experiments have achieved a high muon-tagging efficiency with their muon veto, but the coincidence analysis ultimately depends on the capacity of the detector to be sensitive to Compton scattering and electron tracks while being able to contain the gamma background. This will be the subject of the next section. To palliate for a loss of efficiency in tagging muon induced events in the detector, PMTs could be installed in the water shield to increase the rejection capabilities of external events.

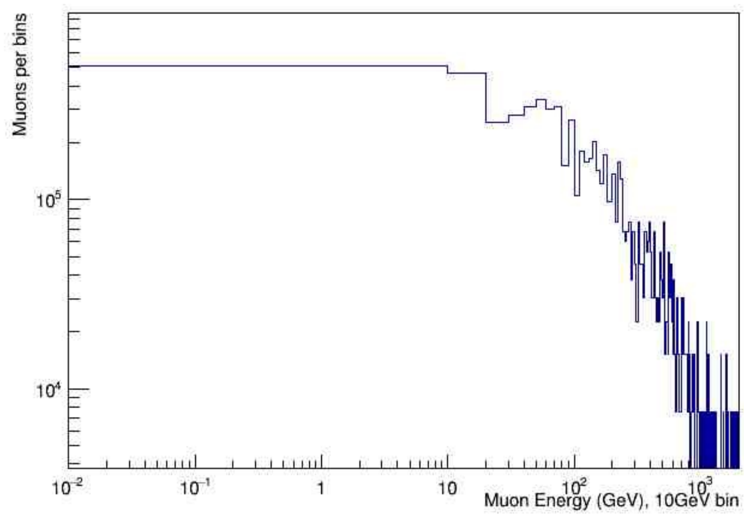

Figure 3: Muon energy spectrum at Boulby using MUSUN

We reviewed the different materials available for the construction of a large vacuum vessel. Ultra-high purity stainless steel and titanium vessels with concentration of radio-nuclei < 100ppt but we found that considering the required mass the vessels, these concentrations are still not enough to be used without internal shielding. The SNO+ collaboration has achieved concentrations of radio-nuclei in acrylic about 10 time lower than the concentrations in the purest steel and titanium we considered during this study, making acrylic the current material of choice to build large dark matter TPC experiments.

We found that the choice of readout strategy greatly impacts on the internal neutron rate. Overall, no readout technology is currently standing out as the best option with regard to its neutron background. In each case, shown in 9 to 11, at least one material was producing too much neutron background. There may be several approach to this problem. Firstly, our simulation relies on an estimate of the quantity of each material inside a detector like CYGNUS. It may be possible to either reduce the required quantity of problematic materials through careful design and planning. Alternative materials may be investigated or higher purity versions of the same materials may be developed. This is particularly relevant to the $\mu-$pic and GEMs options for which better refined glass polymids are being developed and GEMs with high purity G10 insulator instead of kapton are being investigated. [can I say by some of the authors, to account for the different CYGNUS R&D projects ?] In the case of ceramics for the wire readout strategy, it may also be possible to shield the pre-amplifier, or eventually move them outside of the vessel in order to further reduce the neutron background.

0.3 Gamma Backgrounds

In the previous section, we showed that the neutron background can be mitigated by the careful selection of radio-pure materials. The associated gamma background required different shielding technique. For example, the detector can be shielded from the gamma background originating from the rock by building a Lead castle. However, this new element would also contribute to the neutron background. TPCs can be made insensitive to their gamma background as demonstrated in [Ref arXiv:1701.00171] by raising the threshold such that the smaller $^{dE}/_{dx}$ for electron tracks does not trigger the analysis. This technique can be used for CYGNUS at the cost of efficiency and sensitivity to low mass WIMP recoils. Another

Material	Neutron background $\left(\text{year}^{-1}\right)$	Gamma background $\left(\text{year}^{-1}\right)$
Rock		
Vessel (acrylic)	0.138 ± 0.001	$(2.805 \pm 0.002) \times 10^7$
Glass Polymid	$(3.89 \pm 0.02) \times 10^4$	

Table 9: Neutron and Gamma background for $\mu-$pics readout between $1-100$keV

Material	Neutron background $\left(\text{year}^{-1}\right)$	Gamma background $\left(\text{year}^{-1}\right)$
Rock		
Vessel (acrylic)	0.138 ± 0.001	$(2.805 \pm 0.002) \times 10^7$
Copper	< 1.36	$(4.702 \pm 0.002) \times 10^7$
Kapton	22.4 ± 0.1	$(2.515 \pm 0.001) \times 10^8$

Table 10: Neutron and Gamma background for GEMs readout between $1-100$keV

technique is to use the full $3-$D potential of certain readouts such as CCD cameras. This approach, developed in [Ref arXiv:1703.09883 and arXiv:1510.02170], relies on the low threshold of the CCD cameras to veto electron tracks based on the different shape of the Bragg curves for example. The problem with this techniques lies again in the balance between the rate of neutron and gamma backgrounds. We found that pixelated readouts contain a large amounts of heavy metals and other components with a typically large concentration of ^{238}U and ^{232}Th.

In this section, we report on the simulation of the gamma background in the different materials relevant to CYGNUS. Using Geant4, we homogeneously populated the rock, vessel, and sheets of readout materials with ^{238}U,^{232} Th and ^{40}K at rest. Geant4 will automatically simulate the decay chains of the different isotopes with the correct branching ratio. For materials with relatively small thicknesses, such as the vessel or readouts, the homogeneous distribution of the isotopes allows for the simultaneous simulation of bulk and surface background. In the case of the rock, a simulation similar to the one described in 1 showed that only the first 30cm of rock contributes to the gamma background. Beyond this distance, the self-shielding capabilities of the rock are sufficient to stop radiation from leaking.

0.4 Radon and Radon Progeny Backgrounds

Radon gas emanating from materials is a major source background for rare events experiments. In particular, the low energy ($\sim$ 100keV) of radon progeny recoils (RPRs) can mimic a WIMP interaction. ^{222}Rn being a noble gas, its low chemical reactivity makes it particularly difficult to deal with. Moreover, its 3.8 day half-life allows it to spread from the materials where it is produced, making radon a widespread source of background. α-decays of gaseous radon inside the fiducial volume can easily be identified if the associated alpha particle is fully contained. RPRs occurring in the bulk or surface of materials may prove harder to reject. In this case, the associated alpha particle may not be detected, if for example it remains trapped inside the materials. For these surface events, it is possible for a daughter nuclear recoil

Material	Neutron background $\left(\text{year}^{-1}\right)$	Gamma background $\left(\text{year}^{-1}\right)$
Rock		
Vessel (acrylic)	0.138 ± 0.001	$(2.805 \pm 0.002) \times 10^7$
Steel wires	$(2.26 \pm 0.01) \times 10^{-2}$	$(7.583 \pm 0.003) \times 10^4$
Ceramics	86.3 ± 0.3	$(2.11 \pm 0.01) \times 10^8$

Table 11: Neutron and Gamma background for MWPCs readout between $1-100$keV

to enter the amplification region and be recorded as a signal, if the associated alpha particle is not detected, this event constitute a background to the dark matter search. Many efforts from directional detectors have been directed to study and control radon background. In particular, an important mitigation effort was done by the DRIFT collaboration [ref Steve paper on radon arXiv 1407.3938, can include E. Miller cathode paper] to measure and limit radon emanation in the detector. The MIMAC group [ref 1504.05865] also has demonstrated successful detection of radon events. An analysis cut based on the z-position of the events was used to reject RPRs originating from the anode and cathode, where RPRs are an important background due to the high U and Th concentration of Micromegas PCBs.

If the detector is composed of back to back TPCs, cathode-crosser events are unambiguous traces of radon and can be vetoed based on the time coincidence of the charge deposition in both sides of the detector. These events can be used to estimate the level of radon present in the detector as done in [same papers DRIFT + MIMAC]. In DRIFT, these events are vetoed by reducing the fiducial region such that any events detected less than 2cm away from the cathode are rejected [Ref ArXiv1701.00171]. The size of this region is affected by the diffusion of the minority peaks which lowers their amplitudes and hinders the z-reconstruction capabilities of the detector. Furthermore, the precision of the extrapolation of a z position also depends on the time separation of the minority peaks [ref DPSI arXiv1308.0354], better results are obtained when using the P-peak due to its larger separation with the main peak. In this case, the z-resolution is 0.33cm.

Using Geant4, we simulated the range of ^{222}Rn decays and RPRs in CYGNUS. Considering that ^{220}Rn in negligible compared to ^{222}Rn, we simulated a fixed source of ^{222}Rn placed inside the fiducial volume of detector filled with 50Torr of SF_6 as in the previous simulations. Since we are only interested in the range of the nuclear recoils, there is no need to populate the gas homogeneously with ^{222}Rn and the same information can be deduced from a fixed source simulation. Secular equilibrium is assumed throughout the decay chain. The purpose of this simulation is to test the validity of a cut placed 2cm away from the cathode to reject cathode RPRs as described above for the DRIFT detector. The cathode RPR rate we used for CYGNUS is inferred by the rate observed in DRIFT as 3.4 ± 0.4events/day/m^{2}of cathode. 4 shows the full range of the events recorded in the simulation. The z resolution function measured in [ref DPSI arXiv1308.0354] is then applied to the simulated recoil range by adding a random number sampled from a Gaussian distribution with mean 0 and variance 0.33cm to the simulated z-range. Finally, by integrating the smeared distribution of z-ranges, the estimated RPRs rate with a z-range above 2cm can be estimated at 2.57×10^{-16}events/day (90%CL).

While these results would justify the position of the cut at 2cm, many of the parameters used were borrowed from the DRIFT detector. If the existence of minority carriers in SF_6 is proven to be usable, the different resolution of the minority peaks will most likely provide different results.

0.5 Surface and other Backgrounds

0.6 Comparison of Technologies for low background

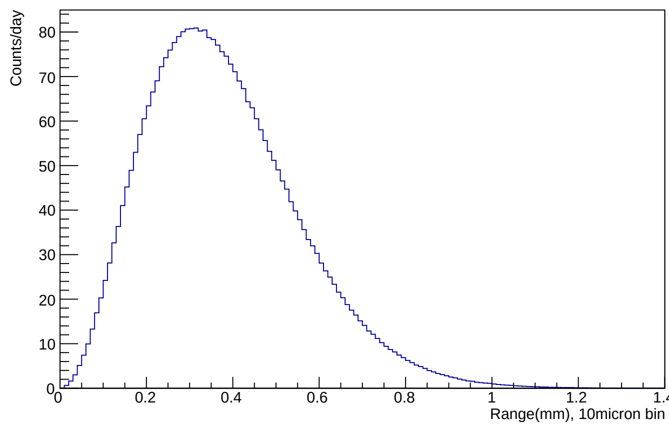

Figure 4: Simulated range of RPRs in 50Torr of SF_6